Journal of Sedimentary Research

Journal of Sedimentary Research, 2012, v. 82, 859–870
Research Article
DOI: 10.2110/jsr.2012.77

PATTERNS OF SEDIMENTATION IN THE CONTEMPORARY RED SEA AS AN ANALOG FOR ANCIENT CARBONATES IN RIFT SETTINGS

SAM J. PURKIS,[1] PAUL M. (MITCH) HARRIS,[2] AND JAMES ELLIS[3]

[1]*National Coral Reef Institute, Nova Southeastern University, 8000 North Ocean Drive, Dania Beach, Florida 33004, U.S.A.*
[2]*Chevron Energy Technology Company, 6001 Bollinger Canyon Road, D-1212, San Ramon, California 94583, U.S.A.*
[3]*Ellis GeoSpatial, 1839 Ygnacio Valley Road, #229, Walnut Creek, California 94598, U.S.A.*
e-mail: purkis@nova.edu

ABSTRACT: **Patterns of sedimentation in the Red Sea offer a contemporary analog for carbonate deposition in marine rift settings. Covering 20° of latitude, the sea is sufficiently long to display pronounced climate differences and the clear tropical waters support vigorous coral reef growth and associated production of carbonate sediment. Six focus areas within the Red Sea, each covering exactly 1,600 sq. km, illustrate the variability of spatial patterns in reefal and other carbonates in this rift setting. Five of the focus areas are located on a north–south transect along the western margin of the sea: (1) Gubal Straits (Egypt), (2) Shalatayn (Egypt), (3) Trinkitat (Sudan), (4) Dahlak (Eritrea), and (5) Halib (Eritrea); and one is from the eastern margin: (6) Farasan Banks (Saudi Arabia). Using Landsat imagery, water depth and two marine facies classes, "reefal frameworks" and "sediments," were mapped. Lumping these two classes define "carbonate bodies" that were analyzed for trends in orientation, relation to local fault networks, and size-frequency distribution. Fault lineaments digitized from the literature are closely related to the orientation of carbonate bodies with areas exceeding 5 sq. km. Smaller bodies do not preferentially align with fault trends. Water depth and the occurrence of reefal frameworks and sediments for the six focus areas are not systematically related. Used as an analog, these data from the contemporary Red Sea may provide insight into the orientation and scale of accumulation of carbonates in subsurface marine rift settings.**

INTRODUCTION

Cutting NNW to SSE across a Precambrian shield, the Red Sea covers 20° of latitude. This basin is sufficiently long to display pronounced climate differences, driven by increased monsoonal influence of the Indian Ocean that creates a north–south gradient in aridity. The clear tropical waters of the Red Sea support vigorous coral reef growth and associated production of carbonate sediment. Miocene and younger carbonate successions in this area attain thicknesses of 450 m (Bosence 2005). The Red Sea is an active rift system; spreading began in the late Oligocene and evolved from a series of continental lacustrine depressions into today's 2,200 m deep marine trough.

Carbonate-dominated marine rifts are common in the geological record, as rift basins provide many shallow-water sites for the establishment of carbonate platforms (Cross and Bosence 2008; Bosence 2012). Receiving only sparse attention in the literature, few well-documented ancient examples exist, however, where platform geometry and shallow marine carbonate facies distribution can be shown to be controlled by rift-related faulting. One example comes from the mid-Miocene Gulf of Suez rift. Here, the geometry of carbonate accumulation is governed by extensional fault-block topography (Burchette 1988; Cross et al. 1998; Cross and Bosence 2008). In this system in onshore Egypt, structural control is imparted predominantly by marginal half-grabens. Dorobek (2008) reviews several Tertiary and Mesozoic examples of syn-rift to early post-rift platforms, where extensional faults control morphology, orientation, and stratigraphy of carbonates.

Given the relatively few ancient examples to illustrate styles of carbonate sedimentation under conditions of extensional tectonism, the Modern Red Sea is interesting in that it may offer conceptual models that can be extrapolated to yield a better understanding of rift-type basins in general, and especially their economically important sedimentary fills and possible reservoir distribution. Fault-block carbonate platforms also represent important hydrocarbon producing reservoirs themselves (e.g., Erlich et al. 1990; Erlich et al. 1993; Grötsch and Mercadier 1999; Fournier et al. 2005; Bosence 2012). The Red Sea potentially represents a modern analog for early and post-rift marine carbonate sedimentation. The aim of this manuscript is to use the Modern Red Sea to explore local and regional controls on shallow-water carbonate facies geometry in an extensional tectonic setting. The results of this study quantitatively illustrate spatial patterns that could provide insight into the geometry and scales of accumulation of carbonate bodies in subsurface analogs.

BACKGROUND

The Red Sea coast is characterized by an almost uninterrupted belt of fringing reefs, as well as barrier reefs and even atolls. Effectively lacking a continental shelf, spectacular steeply sloping drop-offs restrict shallow-water carbonate production to small surface areas. Sediment is almost exclusively skeletal. Below the euphotic zone, carbonate production takes the form of *Globigerina*-rich marl and deepwater limestone (Hofmann et al. 1998; Bosworth et al. 2005). Fringing reefs grow close to the mainland with first-order control on their arrangement and orientation imparted by the tectonic grain of the Red Sea rift (Dullo and Montaggioni 1998; Bosence 2012). Secondary control is exerted by siliciclastic input from the hinterland. Fringing reefs, for example, are typically absent in wadi

Published Online: November 2012

mouths (Braithwaite 1982; Montaggioni et al. 1986; Turak et al. 2007), but not always so (Gvirtznam et al. 1977; Dullo and Montaggioni 1998). Barrier reefs and atolls become more prevalent in the central, and particularly the southern, portions of the basin (Bantan 1999; Reinicke et al. 2003; Rowlands et al. 2012). The Farasan Archipelago, on the eastern margin of the sea, and its western-margin counterpart, the Dahlak Archipelago, both sit atop broad shallow shelves that extend hundreds of kilometers out towards the deep central axis of the rift. The development of offshore reefs is particularly pronounced in these archipelagos, whereas fringing reefs become stifled by siliciclastic influence. Though far offshore from the coast, the reef-crest outlines and the orientation of foreslopes for these buildups, like the nearshore fringes farther north, broadly follow the tectonic framework of the rift (Dullo and Montaggioni 1998). The 9,600 sq. km of Landsat mapping conducted for this study allow a detailed examination of the arrangement of carbonate facies from the northern to southern limits of the Red Sea.

QUANTITATIVE METHODS

Satellite Mapping of Facies

This study employs Landsat 7 ETM+ data to image six 1,600 sq. km focus areas distributed along the eastern and western margins of the Red Sea (Fig. 1). These locations encompass the latitudinal range of shallow-water carbonate deposits in this basin. Three of the six focus areas (Gubal Straits, Dahlak, and Halib) have offshore islands. The remaining three (Shalatayn, Trinkitat, and Farasan) do not.

There is a long lineage of using satellite remote sensing for mapping the arrangement of spectral lithotopes in the Red Sea (Bantan 1999; Purkis et al. 2002; Purkis and Pasterkamp 2004; Purkis et al. 2010; Harris et al. 2012; Rowlands et al. 2012). Segmentation of the Landsat imagery into lithotopes—interpreted to be distinct bodies of uniform sediment—was achieved using a combination of edge detection, spectral and textural analysis, and manual editing. A facies map for each focus area was generated by assigning lithotopes to one of four classes; reefal frameworks (= primarily boundstone), sediments (= skeletal grainstone), emergent (= siliciclastic and/or carbonate), and deep water (= basinal mud) (Figs. 2, 3). This assignment was conducted manually and, following Harris and Vlaswinkel (2008), color, texture, shape, and context relative to other facies were the objective reproducible criteria used to assign each lithotope into a facies class. This attribution was conducted using the object-based image-analysis software eCognition. This method of facies mapping is subjective, so care was taken to maintain consistency in the attribution process and to test for repeatability.

Mapping was first conducted for the three focus areas (Farasan, Dahlak, and Gubal) where seabed maps were available for all or part of the focus area. The map of Farasan was validated against the biotope maps of Rowlands et al. (2012), the map of Dahlak against Carbone et al. (1998), and the map of Gubal against Hamouda and El-Wahhab (2012). Knowledge from these focus areas was used to guide facies mapping in the three remaining focus areas, which lacked independent information. Resultant maps from all six focus areas were further checked against ultra-high-resolution QuickBird (2.4 m pixel) or WorldView-2 (1.8 m pixel) satellite images tendered by Google Earth and against geospatially registered United Kingdom Hydrographic Office (UKHO) nautical charts. As was the case with Rankey (2002) and Harris and Vlaswinkel (2008), it was not possible to measure classification accuracy quantitatively (cf. Purkis and Pasterkamp 2004). Qualitative inspection, however, suggests that the maps truthfully capture the facies arrangements of the six focus areas.

Given that emergent areas are spectrally distinct from submerged areas in the infrared wavelengths (Landsat bands 5–7), it can be expected that facies class "emergent" to be close to 100% accurate. Simultaneous inspection of the blue and red Landsat channels (bands 1 and 3) can reliably be used to identify pixels that do not contain a spectral contribution from the seabed (blue band), but are also unaffected by turbidity (red band). Hence, facies class "deep water" should also be close to 100% accurate. Prediction of accuracy for the attribution of "sediments" and "reefal frameworks" is less straightforward inasmuch as the spectral difference between the two is less dramatic than for emergent and deep-water areas. This said, when viewing an RGB image composed of Landsat bands 1, 2, and 3, the two facies can be clearly distinguished (Harris and Vlaswinkel 2008). Sediments are highly reflective and, in the imagery, can be recognized by their homogeneous white color and visible bedforms. By contrast, reefal frameworks are less reflective, honey-brown to green in color, and have more angular geometries. In lieu of these pronounced differences, a high degree of confusion between classes "sediments" and "reefal frameworks" is not anticipated for the six facies maps.

Prior to analysis, facies classes "sediments" and "reefal frameworks" were lumped to deliver an extra map category, "carbonate facies." From here forward, discrete units of the "carbonate facies" category are termed "carbonate bodies."

Although the maps could be compared qualitatively, a suite of morphometric parameters were extracted from GIS shape files for the carbonate bodies. Data were then quantitatively analyzed for trends and patterns.

Quantifying the Relationship in Orientation of Carbonate Bodies and Fault Lineaments

To quantitatively examine trends, orientations of all carbonate bodies were calculated for the six focus areas by fitting an ellipse to each body and by matching first- and second-order moments. The orientation measurement was taken to be the orientation of the major axis of the fitted ellipse (following Haralick and Shapiro 1992).

To ascertain whether the orientation of carbonate bodies is tectonically influenced, fault maps from the literature (Crane and Bonatti 1987, figs. 6, 12, 13, and 14; Bott et al. 1992, fig. 2; Carbone et al. 1998, fig. H1.1; Khalil and McClay 2002, fig. 2) were geospatially registered and the fault lineaments manually digitized in a GIS (Fig. 1). Though various methods were employed by the original authors to produce their fault maps, all consider onshore structural patterns. The literature fault maps are therefore independent from the offshore carbonate bodies, and a valid comparison can be made between the two datasets. For all focus areas apart from Halib, a circular buffer with a diameter of 150 km was centered on the midpoint of each focus area and used to demark faults that would be considered to be associated with that focus area. For Halib, the buffer diameter was increased to 250 km, because 150 km was insufficient to encompass a representative number of faults for this focus area. Faults lying wholly outside the defined buffer zones were discarded from further analysis. A total of 420 of the digitized faults fell within the six buffers, with lengths varying from 1.5 km to 330 km.

For each focus area, the orientation of fault lineaments were grouped into 15° bins and statistically compared with two populations of orientations for the carbonate bodies: those $<$ 5 sq. km in area and those $>$ 5 sq. km in area. This quantitative comparison was conducted using the parametric Watson-Williams multi-sample test for equal means, which can be used as a one-way ANOVA test for circular data (Mardia and Jupp 2000). As applied, the null hypothesis of the Watson-Williams test is that the means of the orientations of the fault lineaments and tested population of carbonate bodies are equal. If the null hypothesis is upheld for a given focus area at the 95% confidence interval (CI), fault control on the orientation of the carbonate bodies can be concluded. Accordance between the faults and carbonate bodies for each focus area was also visually compared by plotting their orientations in polar coordinates (Fig. 4).

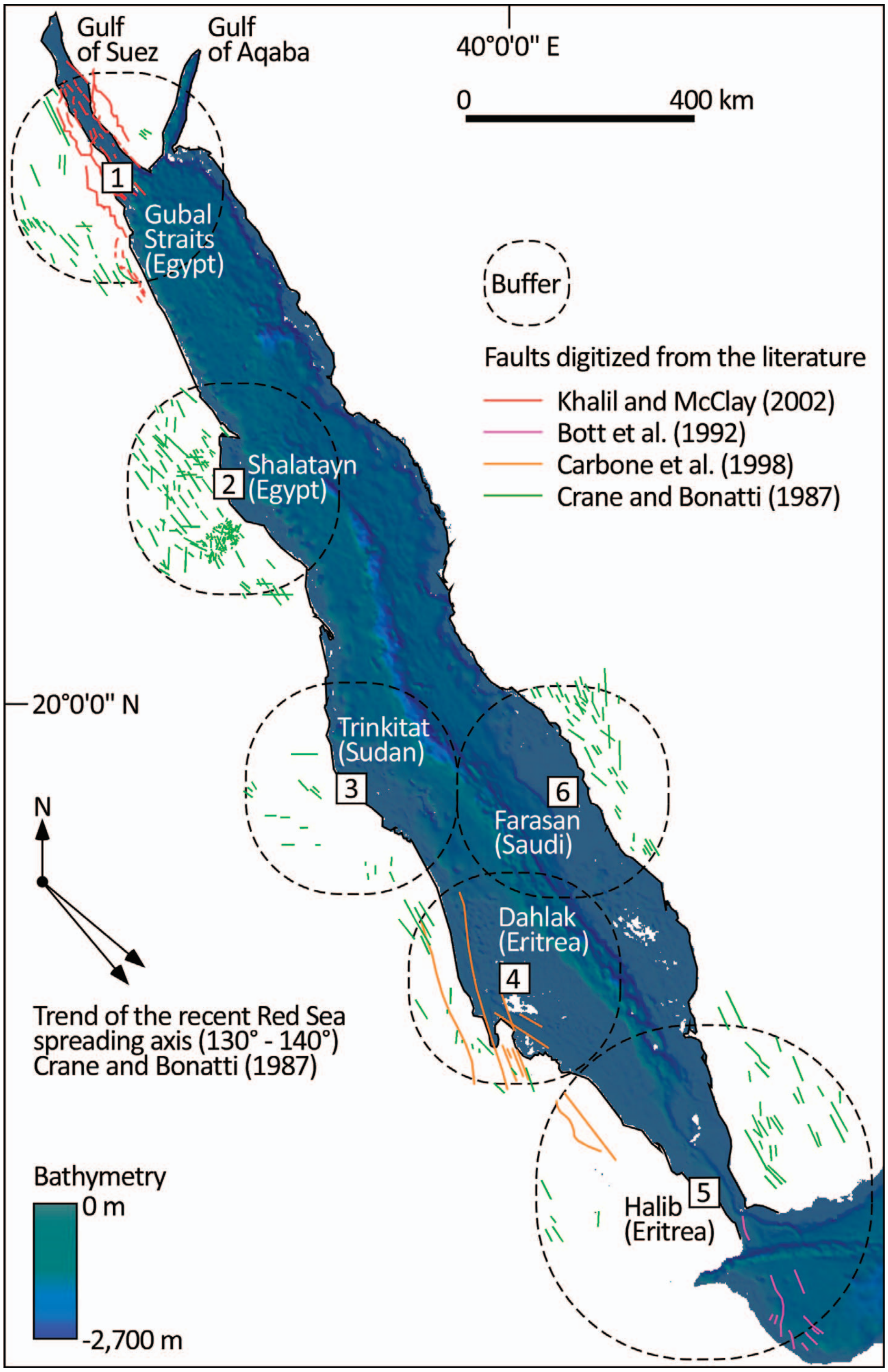

FIG. 1.—Location of the six focus areas distributed down the length of the Red Sea rift. The size of each area is 1,600 sq. km. Fault lineaments surrounding each focus area were digitized from the literature (Crane and Bonatti 1987, figs. 6, 12, 13, and 14; Bott et al. 1992, fig. 2; Carbone et al. 1998, fig. H1.1; Khalil and McClay 2002, fig. 2). For all focus areas apart from Halib, a circular buffer (broken lines) with a diameter of 150 km was used to demark faults that would be considered to be associated with that focus area. The buffer diameter was increased to 250 km for Halib. Color-coded bathymetry from NGDC ETOPO2 Global 2' Elevations.

Quantifying Size-Frequency Distributions and Lateral Extent of Carbonate Bodies

The size-frequency distributions and lateral (planform) extent of carbonate bodies for the six Red Sea focus areas might provide insights to patterns in subsurface analogs. Trends between the frequency of occurrence of carbonate bodies versus their area were explored using the complementary cumulative distribution function (ccdf) $P(X \geq x)$, which is the standard way of visualizing this kind of data (Clauset et al. 2009). Plotted as such, the y axis reports on the probability that a carbonate body is greater than or equal to a given area value (x axis) (Fig. 5).

For each focus area, "width maps" were generated which use color to describe the minimum distance from any point within each carbonate body to the periphery of that body (Fig. 6). The purpose of generating width maps is to highlight between-site differences in the lateral continuity, an important component of geometry, of carbonate bodies.

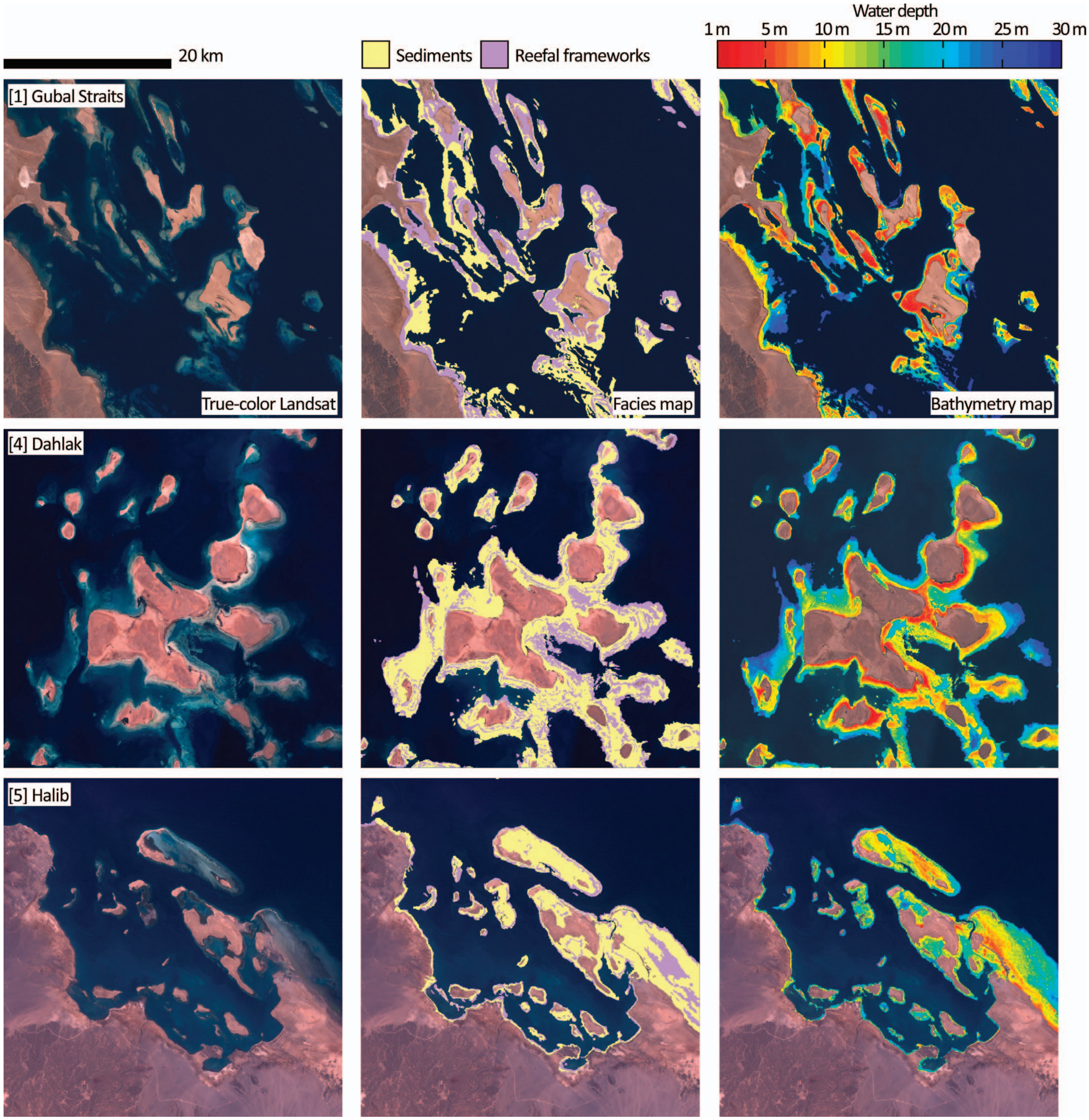

FIG. 2.—Landsat image, facies, and bathymetry maps for the three focus areas with islands (Gubal Straits, Dahlak, Halib). Credit: Landsat courtesy of U.S. Geological Survey.

Satellite Mapping of Bathymetry

Comparison of contrast-stretched Landsat images with UKHO nautical charts indicate that the deepest areas where seabed character could be discerned correspond to a water depth of 30 m, which is consistent with visible-light penetration in the tropical waters of the region (Bosscher and Schlager 1993; Purkis et al. 2002; Purkis and Pasterkamp 2004). Facies mapping was therefore conducted only down to 30 m water depth, with all remaining non-emergent portions of the imagery assigned to the "deep water" class and discarded from further analysis. Following the ratio-algorithm method of Stumpf et al. (2003), depth soundings digitized from UKHO nautical charts were used as training data to tune the coefficients of the algorithm, and spectral bathymetry was extracted from the Landsat. Digital elevation models (DEMs) were constructed for each focus area. These DEMs capture seabed topography from the low-water mark to 30 m water depth and have a spatial resolution of 30 m^2, that of the Landsat imagery from which they were derived. The DEMs were produced so as to assess the

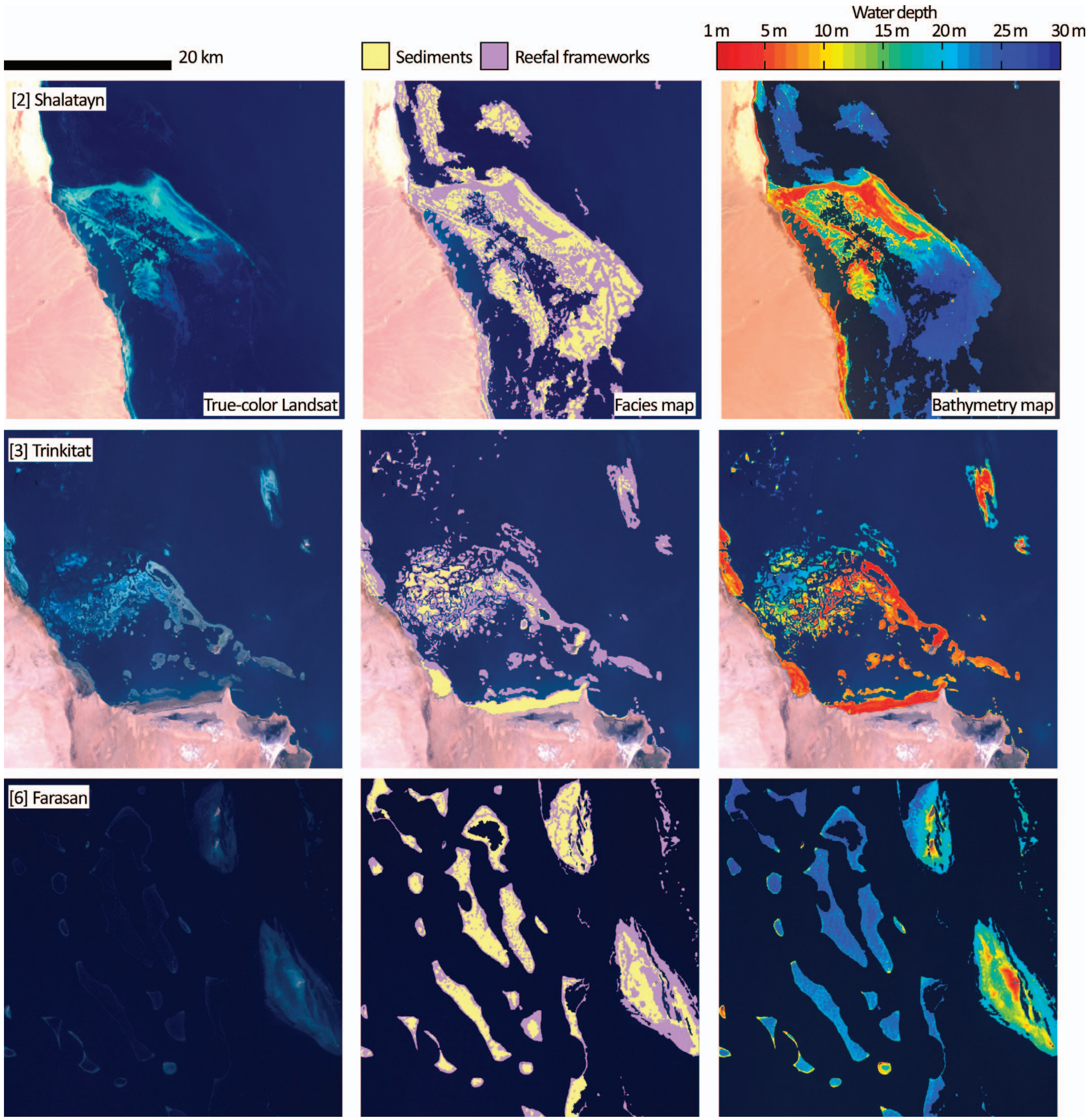

FIG. 3.—Landsat image, facies, and bathymetry maps for the three focus areas without islands (Shalatayn, Trinkitat, Farasan). Credit: Landsat courtesy of U.S. Geological Survey.

arrangement of the mapped facies classes with respect to water depth, as has been conducted previously for modern shallow-water carbonate depositional systems (Wilkinson et al. 1999; Rankey 2004; Purkis et al. 2005; Harris and Vlaswinkel 2008; Bosence 2008; Purkis and Vlaswinkel 2012).

To explore relations between water depth and the two shallow-water facies classes, "reefal frameworks" and "sediments," the mean depth for each mapped patch (polygon) for these two facies was calculated for each of the six focus areas. This was achieved by tallying the values of the DEM subtended by each patch for the two facies classes and averaging to yield a mean. For each water depth, abundance was calculated as the number of occurrences of each class divided by the total number of patches at that water depth (Fig. 7).

Following Rankey (2004) facies diversity (*H*), at any given water depth can be quantified using the Shannon–Weaver diversity index (Shannon and Weaver 1962). This metric estimates the uncertainty in predicting

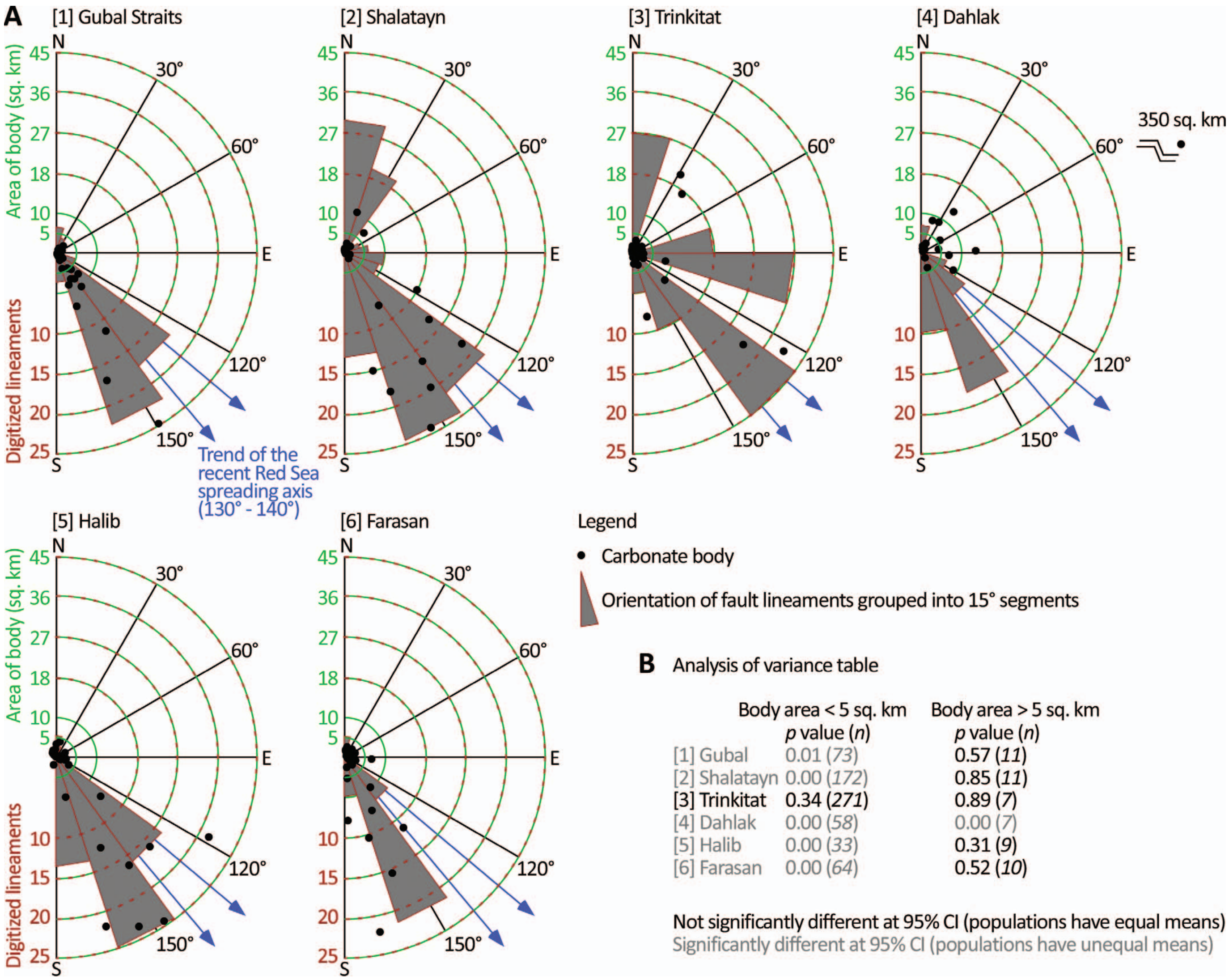

FIG. 4.—**A)** Rose diagrams for each focus area in polar coordinates showing frequencies of the orientation of digitized fault lineaments grouped into 15° bins (gray segments) and the orientations of carbonate bodies (black dots). The arrowed blue lines show the trend of the recent spreading axis of the Red Sea rift (Crane and Bonatti 1987). **B)** Analysis of variance table with results from the parametric Watson-Williams multi-sample test for equal means applied to the orientation of the fault lineaments and the orientation of carbonate bodies with areas < 5 sq. km and > 5 sq. km. Non-significant results (black text) represent cases where the mean orientation of the faults is statistically the same as the mean orientation of the carbonate bodies. Significant results, those where the means are statistically different, are in gray text. The number of bodies for each test is given by *n*. The results suggest increasing organization in the orientation of carbonate bodies with increasing size.

abundances of elements (e.g., given a water depth, how much uncertainty is there in predicting facies type?). In the context of this study, given a water-depth range in which there exist two (n) facies classes (reefal frameworks and sediments) with proportions $p_i, \ldots, p_n$ within that water depth range, diversity (H) for each water depth is defined as

$$H = -\sum_{i=1}^{n} p_i \cdot \ln p_i \quad (1)$$

A value of $H = 0$ indicates a perfectly ordered system (a given water depth is characterized by only one facies class; not diverse), whereas higher H indicates a greater number of facies classes (diverse).

As per Rankey (2004), it can be assumed that both facies categories can be represented in all water depths and calculate the maximum possible value of H (termed H_{max}) as ln(n). Divergence from the maximum can then be defined by the Shannon–Weaver evenness index (E):

$$E = 1 - (H/H_{\max}) \quad (2)$$

E ranges from zero ($H = H_{max}$) to one, with E values near unity showing that the system is not diverse ($H = 0$), but instead dominated by one facies class (Rankey 2004).

RESULTS

Analyzing the Relationship between Orientation of Carbonate Bodies and Fault Lineaments

The trend of the recent Red Sea spreading axis lies between 310° and 320° (Crane and Bonatti 1987), equating to 130–140° in the angular units of the polar plots (arrowed blue lines, Fig. 4A). Simple visual examination suggests that the orientation for the majority of faults mapped for the six focus areas can be related to the tectonic grain of the

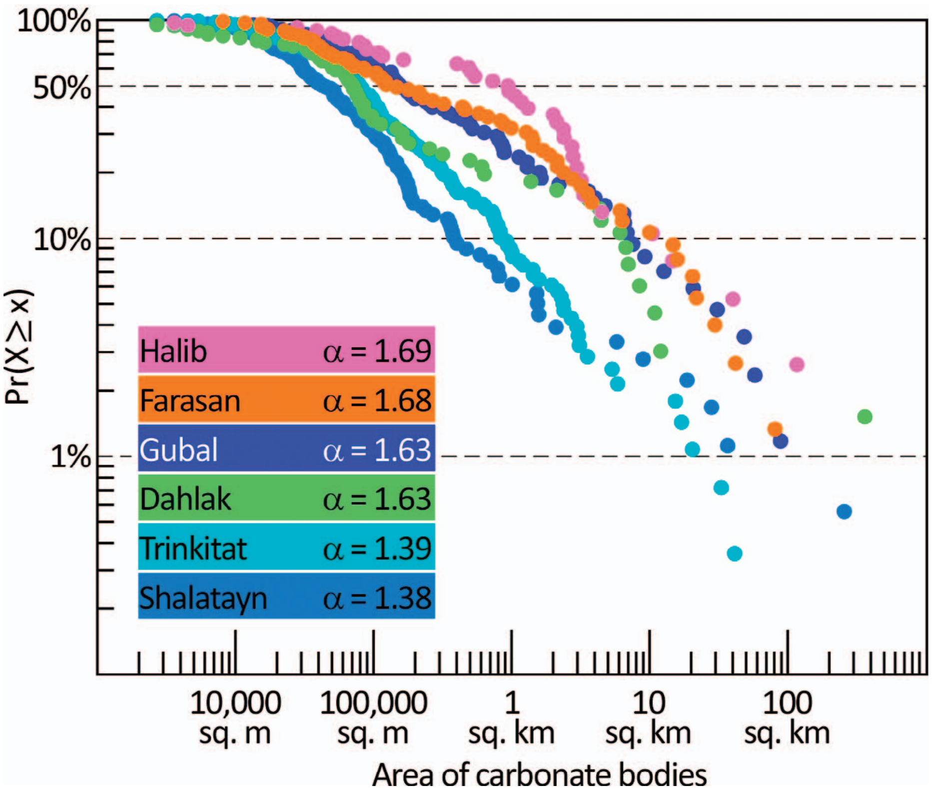

FIG. 5.—Complementary cumulative distribution function (ccdf) $P(X \geq x)$ of the populations of areas for carbonate bodies for the six focus areas. *x*-axis—log body area, *y*-axis—log probability that a body is greater than or equal to a given area value. Linear trend in log-log plot indicates power-law. Under power-law conditions, abundance can always be obtained from area by a constant factor α. Focus areas with islands (Halib, Gubal Straits, Dahlak) have higher α than those without. Farasan is an exception: it lacks islands but reports a high α.

Red Sea rift (Fig. 1). Polar plots of the orientations of the fault lineaments and carbonate bodies indicate varying levels of accordance for the six focus areas (Fig. 4A). Clear trends, however, become apparent after partitioning the carbonate bodies into two groups by area, those < 5 sq. km and those > 5 sq. km, and applying the Watson-Williams test (Fig. 4B). For all focus areas apart from Trinkitat, the mean of the orientations of < 5 sq. km carbonate bodies is significantly different at the 95% CI to the mean of the orientation of the mapped fault lineaments. It can be inferred from this result that Trinkitat is the only focus area in which faults direct the orientation of the "small" carbonate bodies. By contrast, when the carbonate bodies with areas > 5 sq. km are considered, four of the five focus areas show statistically significant accordance between the orientation of the bodies and the fault lineaments; Dahlak is the only focus area to lack such a relationship for these "large" carbonate bodies. As is discussed later, Dahlak is also unique among the six focus areas in terms of its complex arrangement of islands, shallow shelves, and deep troughs, features related to the movement of upper Miocene evaporites.

Analyzing Size-Frequency Distributions and Lateral Extent of Carbonate Bodies

For all focus areas, the abundance of small carbonate bodies is greater than the abundance of large ones (Fig. 5). Further, in the size range of 10,000 sq. m to 100 sq. km, the relationship between decreasing probability of encounter and increasing area is roughly linear for all sites, suggesting power law scaling, which is now a frequently interpreted trend for carbonate facies (Drummond and Dugan 1999; Rankey 2002; Purkis et al. 2007; Purkis et al. 2010; Fullmer et al. 2010). If characteristic of the data, a power-law would suggest carbonate-body abundance to scale as an inverse power to body area. However, a roughly straight trend on a log-log plot is a necessary but not sufficient condition for power-law behavior, and it is necessary to test for two other distributions with similar form: the negative exponential and lognormal. A negative exponential distribution would report carbonate-body abundance to increase exponentially with a linear decrease in carbonate-body area. If the logarithms of the carbonate-body areas were to form a normal distribution, the original (antilog) areas would be lognormally distributed. Lognormal distributions may be almost indistinguishable from power laws (Perline 2005), in that both can result in a nearly straight trend on a log-log plot. Negative exponential distributions differentiate from lognormal and power-law at the small end of the size spectrum, where there is an underrepresentation of small units.

The power-law, exponential, and lognormal are all "heavy-tailed" distributions, meaning that there is a nontrivial amount of weight far from the center of the distribution (Clauset et al. 2007). For the data, this implies that carbonate bodies orders of magnitude larger (or smaller) than the mean are relatively common. As per Clauset et al. (2007), the latter point is particularly true when compared to a normal distribution, where essentially no weight is far from the mean. The salient message from this analysis is not the separation of power-law, exponential, and lognormal behavior, but instead, the result that the plan-view areas of the carbonate bodies are heavy-tailed and hence do not cluster around a typical value. Therefore, simple traditional statistics for normal distributions, such as mean and variance, are poor descriptors of the size-frequency distributions and could not be used to parameterize geostatistical models of the focus areas. This is an important observation, but detailed consideration of how heavy-tailed size-frequency distributions should be imparted to reservoir models is beyond the scope of this report.

To statistically test for the presence of power-law, negative exponential, and lognormal distributions, the three-step procedure of Clauset et al. (2009) was followed. This test reports all six focus areas to be lognormally distributed when the full range of the data is considered. Repeating the test after discarding carbonate bodies with area < 10,000 sq. m (i.e., following Clauset et al. 2009, and imposing an $_{x}min$ threshold), which is the point in the six series where the trends "roll" parallel to the horizontal axis, identifies the size-frequency distribution of Shalatayn and Trinkitat

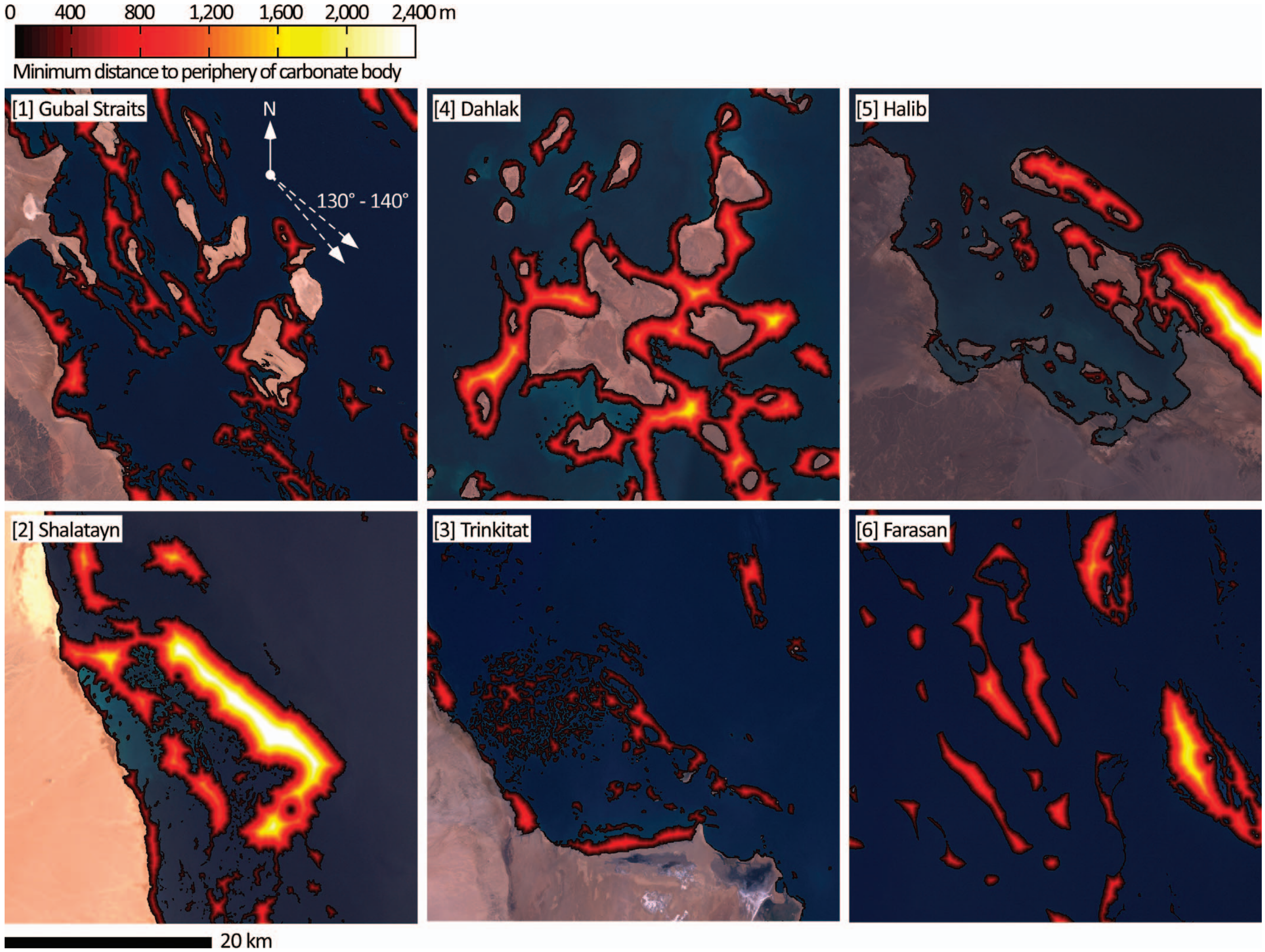

FIG. 6.—Planform width maps of carbonate bodies. Hotter colors demark wider, more laterally expansive, carbonate bodies. Top row are the three focus areas with offshore islands (Gubal Straits, Dahlak, and Halib). Bottom row are the three remaining focus areas which lack islands (Shalatayn, Trinkitat, and Farasan). Dashed white arrowed lines show trend of the recent Red Sea spreading axis (130–140°) (Crane and Bonatti 1987). Credit: Landsat courtesy of U.S. Geological Survey.

as power-law. Distributions of all other focus areas remain classified as lognormal.

It is apparent from the width maps (Fig. 6) that the focus areas with offshore islands (Gubal Straits, Dahlak, and Halib) do not display more laterally extensive bodies than those which lack islands (Shalatayn, Trinkitat, and Farasan). For instance, the largest carbonate body mapped for Shalatayn, a focus area without islands, is as laterally extensive as that of Halib, where islands are present. For both, the largest bodies attain widths exceeding 5 km.

One mechanism by which islands may influence the lateral extent of carbonate bodies is by serving as nucleation points from which carbonate deposition can build out. However, relevant too is the depth to underlying bedrock, inasmuch as it controls water depth. The potential of a system to prograde is dictated by water depth, amongst other factors, and deep separating channels can prevent, or at least delay, the coalescence of two adjacent carbonate bodies. Three focus areas, Gubal Straits, Trinkitat, and Farasan, are notable for their limited width of carbonate bodies. The first (Gubal Straits) has islands. The other two do not. The width maps for the three focus areas show abundant channels incising the depositional systems, and the DEMs inform these channels to exceed 30 m water depth (Figs. 2, 3). Here, it appears that water depth, not the absence of islands, is the factor presently limiting shallow-water carbonate deposition.

Analyzing the Relationship between Water Depth and the Occurrence of Reefal Frameworks and Sediments

Even a cursory glance at the distribution in abundance of the facies classes "reefal frameworks" and "sediments" with water depth illustrates that both classes occur across a range of water depths (Fig. 7). Beyond the raw count data, however, Shannon–Weaver entropy metrics provide quantitative information on diversity and describe its structure for the six focus areas (Table 1). The Shannon–Weaver diversity index (H) is high for all focus areas, indicating high diversity of the two facies classes with water depth. The lack of partitioning between facies is further reinforced by the Shannon–Weaver evenness index (E). In the situation where E approaches 1, there is a more deterministic relationship: given a water depth, the occurrence of a facies class can be confidently predicted. E is proportional to the percentage that uncertainty has been reduced from the maximum. Taking Halib as an example, for a given water depth, the value of E = 0.09 means that the observed uncertainty in facies-class occurrence has been reduced 9% relative to the maximum possible

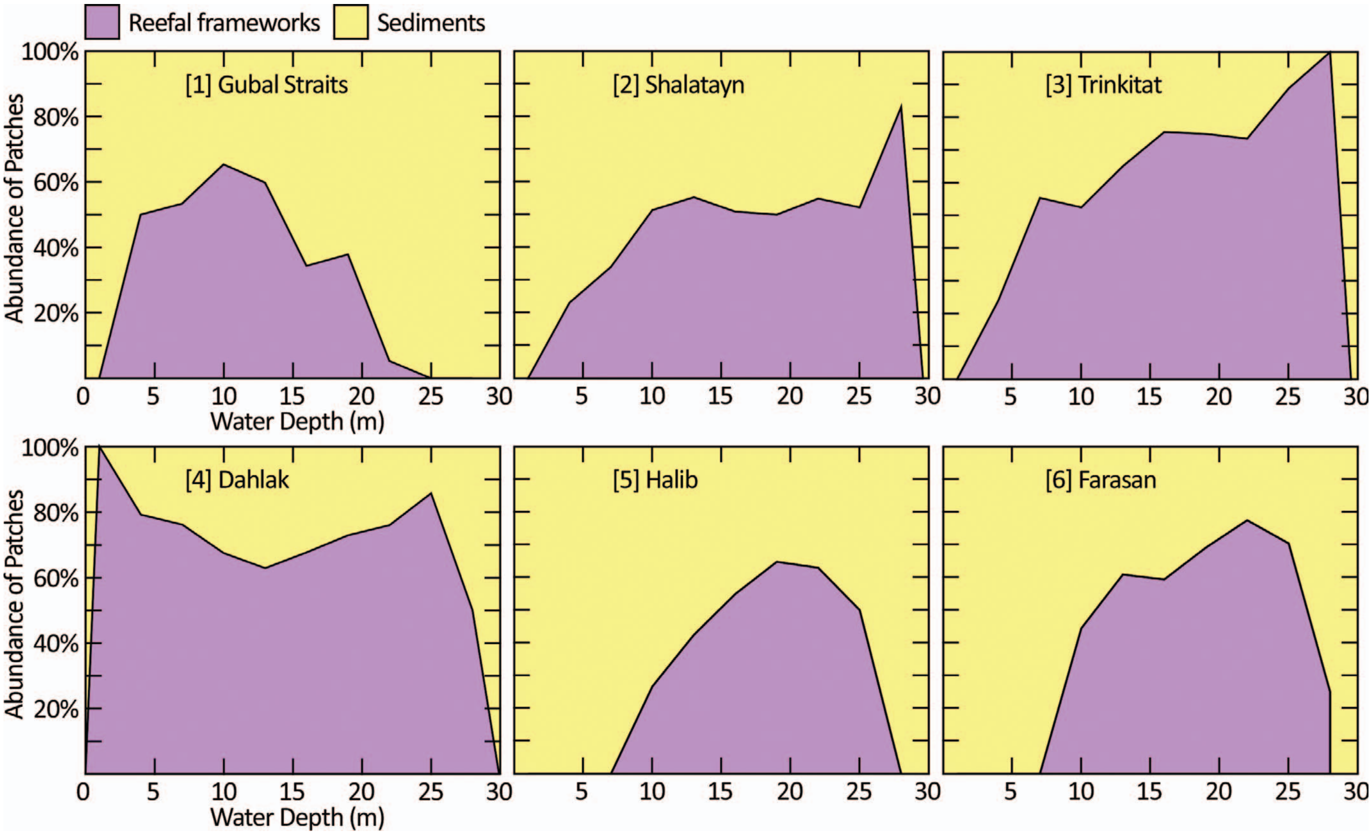

FIG. 7.—Abundance of patches (%) for each water depth for facies classes "reefal frameworks" and "sediments." For each water depth, abundance was calculated as number of occurrences of each class divided by the total number of patches at that water depth. Both classes are present across a wide range of water depths.

entropy and, conversely, that there is a 9% deterministic or predictable component, as constrained by water depth. This value clearly represents a low degree of predictability and is in line with the equal or lower values of *E* returned for the five focus areas (Table 1).

DISCUSSION

The Relationship between Orientation of Carbonate Bodies and Fault Lineaments

Investigation into the degree of influence of local fault trends on the orientation of carbonate bodies (a combined class encompassing areas mapped as sediments and reefal frameworks) reveals relationships that can be related to the body sizes. Small bodies, those $<$ 5 sq. km in area, are far more prevalent in the landscapes than large ($>$ 5 sq. km) (Fig. 5) and statistically show little to no accordance in orientation with the mapped fault lineaments (Fig. 4). With the exception of Dahlak, the less numerous bodies of area $>$ 5 sq. km, instead, are statistically aligned with the mapped faults (95% CI). It can be concluded that the six focus areas contain a myriad of small depositional units with random alignment and a few more laterally expansive units, sufficiently large to be structurally relevant in a hydrocarbon exploration context, that have a statistical tendency to align with the direction of local faults. Local faults for each of the six focus areas are also broadly aligned to the trend of the recent Red Sea spreading axis (Fig. 1). The logical extension of these results to the subsurface is, that if the Red Sea can be considered an appropriate analog, broad knowledge of the orientation of the spreading axis in a rift setting can be used to inform on the likely orientation of carbonate bodies with areas $>$ 5 sq. km.

TABLE 1.—*Shannon–Weaver diversity index (*H*) and Shannon evenness (*E*) of water depth for the distribution of facies classes "reefal frameworks" and "sediments" for the six focus areas. Low values of* H *mean that that one of the two classes occurs over a limited range of water depths; low values of* E *suggest that neither class is distributed by water depths in a manner that is any different than that expected for the maximum possible entropy.*

Focus Area	*H*	*E*
[1] Gubal-Straits	2.21	0.04
[2] Shalatayn	2.89	0.02
[3] Trinkitat	2.75	0.09
[4] Dahlak	2.76	0.03
[5] Halib	2.10	0.09
[6] Farasan	2.10	0.09

Dahlak is an important exception inasmuch as here, the presence of large, numerous, and closely spaced offshore islands seems to exert primary influence on the orientation of the carbonate bodies. Whereas islands are also present for the Gubal Straits and Halib, they too are broadly aligned to the trend of the spreading axis of the basin (Fig. 6). There is, however, a difference. Dahlak's islands, which are Plio-Pleistocene in age, are situated over salt highs (driven by movement of upper Miocene evaporites) (Bunter and Abdel Magid 1989; Carbone et al. 1998; Orszag-Sperber et al. 1998; Crossley and Cripps 1999). Sitting atop salt diapirs, the islands of the Dahlak archipelago adopt circular, semicircular, and arcuate shapes. It can be interpreted that these complex shapes along with that of the associated submarine topography, the geometries of both related to the movement of salt, serve to exert primary control on the orientation of the carbonate bodies, upsetting the relationship to local faults shown to be present for the other five focus areas.

The carbonate platforms of the Farasan Banks focus area also sit atop salt diapirs (Guilcher 1988). Here, diapiric structures formed submarine highs that have developed into carbonate platforms as they have spent a significant amount of time in the shallow-water carbonate production zone (Bosence 2012). Such platforms are termed salt diapir platforms (Bosence 2005) and adopt circular, arcuate, amoeboid, and elongate shapes, punctuated with subcircular embayments and deep reentrants and channels (Rowlands et al. 2012). Despite the influence of salt diapirism, and unlike Dahlak, the influence of the direction of local faults on the orientation of carbonate bodies in the Farasan Banks is the same as for the majority of the focus area; bodies with area $<$ 5 sq. km are not directed by the faults, and the $>$ 5 sq. km bodies preferentially align with them.

The varying influence of faults on carbonate bodies of different sizes may arise for two reasons. The first can be explained in process terms and the second as a statistical artifact. Studies at comparable scale that consider planform geometries of both sand and reefal bodies in modern carbonate depositional environments report large units to be elongate in shape and small units to be rounded (Purkis et al. 2007; Harris et al. 2011). A rounded shape does not have a preferred orientation. The relationship between body size and shape has been explained by the influence of different hydrodynamic and biotic processes acting on carbonate bodies less than a few square kilometers in area, versus those acting on larger bodies (Purkis et al. 2007). For example, it can be imagined that the hydrodynamics influencing small bodies to be the same as those of the surrounding waters. Larger bodies may modify the prevailing hydrodynamics and set up local gradients, an effect which conceivably may have biotic ramifications, e.g., in terms of the retention of coral larvae (Pinsky et al. 2012). A statistical artifact may also explain the differential behavior in orientation of small and large bodies. A carbonate body with an area of 5 sq. km consists of $\sim$ 5,500 30 m $\times$ 30 m Landsat pixels, whereas a 1 sq. km body consists of $\sim$ 1,000 pixels and a 0.5 sq. km body of only $\sim$ 270 pixels. A threshold in the number of pixels that comprise a body must exist, below which shape, and hence also orientation, cannot be accurately assessed. A statistical artifact will therefore arise as the resolution of the dataset (1 Landsat pixel = 30 m $\times$ 30 m) is approached. Given that the smallest carbonate body considered in the Red Sea analysis consists of nine Landsat pixels (8,100 sq. km in area), which is a sufficient number to capture the geometry of a body, it is unlikely that the small size of the bodies is preventing orientation from being calculated accurately. The difference in behavior between small and large bodies cannot therefore be easily ascribed to a statistical artifact and should be assumed to be real.

Size-Frequency Distributions of Carbonate Bodies

Power-law trends are scale-invariant across their entire distribution. The abundance (y) of an object, in an inverse power-law distributed population, scales as an inverse power of the size of the object (x). Under these conditions, y can always be obtained by scaling x by a constant factor α, such that $y = x^{-\alpha}$. It is because this relationship holds for all values of the power law that the distribution is said to be scale invariant. Lognormal distributions can be similar in shape to power-law distributions. For instance, if X has a lognormal distribution, then in a log-log plot of the ccdf $P(X \geq x)$, the behavior will appear to be nearly a straight line for a large portion of the body of the distribution. Indeed, if the variance of the corresponding normal distribution is large, the distribution may appear linear on a log-log plot for several orders of magnitude (Mitzenmacher 2003), so called "power-law mimicry" (Perline 2005).

From the perspective of gaining insight into scales of accumulation of carbonates, the scale-invariant property of power-law and lognormal distributions is of interest because it allows the likelihood of occurrence of small bodies in a subsurface system to be computed using the same relationship that exists between the frequency of the large bodies and their size. For instance, under the assumption of power-law, if the large bodies in a system can be resolved by seismic and the small ones cannot, the power in the predictability of the scale-invariant relationship is obvious. However, as illustrated by the different slopes (α) of the ccdf $P(X \geq x)$, there are differences in the relationship between abundance and area of carbonate bodies between the Red Sea focus areas (Fig. 5). For example, for Trinkitat, given an occurrence of a carbonate body, there is a 10% likelihood that the body is $>$ 1 sq. km in size. For Dahlak, Gubal, Farasan, and Halib, there is a 10% likelihood that the body is $>$ 10 sq. km, and so on. These differences become important if the α of the ccdf from a modern analog is to be used to inform on the abundance of bodies of a given size in the subsurface. There is the hint of a relationship between α and the presence (Gubal Straits, Dahlak, and Halib) and absence (Shalatayn, Trinkitat, and Farasan) of islands. Dahlak, the Gubal Straits, and Halib have high α (shallow slopes to their ccdf). Meanwhile, Shalatayn and Trinkitat have noticeably steeper slopes (lower α). Farasan, however, is an exception in being a focus area without islands but a high α. Given this exception and given too that only six focus areas have been considered, it is premature to place any weight on the observation that the focus areas with islands have higher α to their ccdf than the focus areas without islands. Further investigation into the controls on α is required.

The Occurrence of Reefal Frameworks and Sediments is Unrelated to Water Depth

Arrangements of facies versus water depth in the Modern have been published on extensively, and the majority of contributions to the literature have arisen from studies in the tropical Atlantic. Rankey (2004) examined 400 sq. km of seabed offshore of the Florida Keys with a depth range of 1–9 m and concluded a random arrangement of facies with depth. Similarly, Wilkinson et al. (1999) concluded a random patterning for 723,000 sq. km of Florida–Bahamas lithotopes in space; depth was not considered. In the Arabian Gulf, Purkis et al. (2005) also concluded a random ordering of fabrics for a 25 sq. km plot in which facies were mapped for depths spanning 5–7 m. In contrast, by considering 2 sq. km of Florida seabed with water depth ranging from 0–3 m, Bosence (2008) employed embedded Markov chain analysis to identify the relationship of facies to depth to be ordered. It should be noted that the Markov approach of Bosence (2008) is quite different from that of Rankey (2004), who employed metrics to estimate the uncertainty in predicting the abundance of facies elements at different water depths. In a study from the Pacific which spanned water depths of 0–40 m, Purkis and Vlaswinkel (2012) showed several facies to inhabit narrow and well-defined depth regimes, sufficient to be considered non-random, whereas others could not be constrained so precisely. Despite methodological differences, the status quo on this subject hence falls into three camps: a handful of studies that observe random ordering (Rankey 2004; Purkis et al. 2005; Wilkinson et al. 1999), one study which reports deterministic ordering with respect to depth (Bosence 2008), and one study that shows aspects of both randomness and determinism (Purkis and Vlaswinkel 2012).

Investigation into the degree to which facies are diagnostic of water depth was not central to this study, for several reasons. First, limited by the coarse spectral and spatial resolution of Landsat and lacking ground control, we opted to map to only two broad facies classes in the 0–30 m water depth range—"sediments" and "reefal frameworks." The urge to be more ambitious with the number of classes was resisted in order to balance the need for high map accuracy. Second, the optical derivation of the bathymetric DEM for each focus area from the Landsat imagery was guided by several tens of depth soundings digitized from UKHO nautical charts. This approach will not deliver as high an accuracy as when derivation is guided by many thousands of soundings acquired in the field using sonar (cf. Purkis et al. 2010; Rowlands et al. 2012). While we recognize these limitations, the data are sufficient to provide broad insight into the lack of a relationship between water depth and sediments and reefal frameworks in the 0–30 m depth range, at Landsat scale, for the six focus areas. The lack of diagnostic power that water depth provides for the occurrence of the two classes is visually and statistically evident (Fig. 7; Table 1). At most, uncertainty (E), as compared to maximum possible entropy in the water depth to facies relationship, is reduced by 9% (Farasan and Halib), but for all other focus areas E is considerably lower. Following the interpretation of Rankey (2004), this result for Halib and Farasan, both best case scenarios, can be taken to mean that "*if we knew a facies type to be present at a given location, that information would constrain water depth only 9% better than the case in which we merely guessed at water depth at a given location with no other information*." There clearly is no deterministic relation between the two facies types and water depth in any of the six focus areas considered.

For the reefal frameworks, whereas water depth is significant in terms of both mode of life and taxonomy (Bosscher and Schlager 1993), the data show that the clear waters of the Red Sea allow the zone of significant reef growth to extend down to at least the maximum mapped water depth (30 m). If our DEMs and facies mapping extended to greater water depths, as was the case for Purkis and Vlaswinkel (2012), differentiation of facies into water-depth ranges likely would be observed; areas beneath the zone of reef growth would be dominated by sediments. As per Rankey (2004), this point implies that identification of order versus randomness in the arrangement of facies with water depth is dependent on the *range* of water depth considered. Like this study, previous work which reports no pattern between facies and water depth (Rankey 2004; Purkis et al. 2005) have considered narrow depth ranges.

CONCLUSION

The Red Sea provides a classic analog for investigating the interplay between rift tectonics and shallow-water marine carbonate sedimentation. Six focus areas within the Red Sea, each covering exactly 1,600 sq. km, illustrate the variability of spatial patterns in reefal and other carbonates in this rift setting. The orientation of Red Sea carbonate bodies with areas $<$ 5 sq. km is not dominantly (statistically) controlled by faults. The orientation of larger bodies is fault-directed for five of the six focus areas, which encompass the latitudinal range of shallow-water carbonate deposits in the Red Sea, from coastal shelves to diapirically controlled offshore highs. Dahlak is an exception, and in this focus area we interpret the orientation of $>$ 5 sq. km carbonate bodies to be controlled by closely spaced islands, whose geometry is in turn directed by underlying salt diapirs. The presence of islands was not shown to deliver more laterally expansive carbonate bodies for any of the six focus areas, nor was water depth found to be related to the relative abundance of reefal frameworks and sediments. The size-frequency distribution of bodies for all focus areas was shown to be lognormal. This distribution is heavy-tailed, so called because there exists a nontrivial amount of weight far from the center of the distribution. For this reason, a lognormal distribution is not well described by the mean and variance of the population.

ACKNOWLEDGMENTS

We thank Chevron Energy Technology Company for support of this research and for permission to publish. The Landsat tiles came courtesy of the U.S. Geological Survey, and we acknowledge Google Earth for online imagery. The ETOPO2 Global 2' Elevations data used in Figure 1 are from the Research Data Archive, which is maintained by the Computational and Information Systems Laboratory at the National Center for Atmospheric Research (NCAR). NCAR is sponsored by the National Science Foundation. We are grateful to Gwilym Rowlands for sharing his broad knowledge of the Red Sea, to Lotte Purkis for help in preparing the satellite images, and to Jeremy Kerr for statistical assistance. We are grateful for highly constructive and useful reviews returned by Dan Bosence and Marcello Minzoni, as well as for the comments of Associate Editor Peter Burgess and Editor Gene Rankey. This is NCRI publication 150.

REFERENCES

Bantan, R.A., 1999, Geology and sedimentary environments of Farasan Bank (Saudi Arabia) Southern Red Sea: a combined remote sensing and field study [PhD Thesis]: Royal Holloway, University of London, 297 p.

Bosence, D.W.J., 2005, A genetic classification of carbonate platforms based on their basinal and tectonic settings in the Cenozoic: Sedimentary Geology, v. 175, p. 49–72.

Bosence, D., 2008, Randomness or order in the occurrence and preservation of shallow-marine carbonate facies? Holocene, South Florida: Palaeogeography, Palaeoclimatology, Palaeoecology, v. 270, p. 339–348.

Bosence, D., 2012, Carbonate dominated marine rifts, *in* Roberts, D.G., and Bally, A.W., eds., Regional Geology and Tectonics: Phanerozoic Rift Systems and Sedimentary Basins: Amsterdam, Elsevier, p. 89–114.

Bosscher, H., and Schlager, W., 1993, Accumulation rates of carbonate platforms: Journal of Geology, v. 101, p. 345–355.

Bosworth, W., Huchon, P., and McClay, K., 2005, The Red Sea and Gulf of Aden Basins: Journal of African Earth Sciences, v. 43, p. 334–378.

Bott, W.F., Smith, B.A., Oakes, G., Sikander, A.H., and Ibraham, A.I., 1992, The tectonic framework and regional hydrocarbon prospectivity of the Gulf of Aden: Journal of Petroleum Geology, v. 15, p. 211–243.

Braithwaite, C.J.R., 1982, Patterns of accretion of reefs in the Sudanese Red Sea: Marine Geology, v. 46, p. 297–325.

Bunter, M.A.G., and Abdel Magid, A.E.M., 1989, The Sudanese Red Sea, 1. New developments in stratigraphy and petroleum geological evolution: Journal of Petroleum Geology, v. 12, p. 145–166.

Burchette, T.P., 1988, Tectonic control on carbonate platform facies distribution and sequence development: Miocene, Gulf of Suez: Sedimentary Geology, v. 59, p. 179–204.

Carbone, F., Matteucci, R., and Angelucci, A., 1998, Present-day sedimentation on the carbonate platforms of the Dahlak Islands, Eritrea, *in* Purser, B.H., and Bosence, D.W.J., eds., Sedimentation and Tectonics in Rift Basins: Red Sea–Gulf of Aden: London, Chapman and Hall, p. 523–536.

Clauset, A., Young, M., and Gleditsch, K.S., 2007, On the frequency of severe terrorist events: Journal of Conflict Resolution, v. 51, p. 58–87.

Clauset, A., Shalizi, C.R., and Newman, M.E.J., 2009, Power-law distributions in empirical data: SIAM (Society for Industrial and Applied Mathematics) Review, v. 51, p. 661–703.

Crane, K., and Bonatti, E., 1987, The role of fracture zones during early Red Sea rifting: structural analysis using Space Shuttle radar and Landsat imagery: Journal of the Geological Society, London, v. 144, p. 407–420.

Cross, N.E., and Bosence, D.W.J., 2008, Tectono-sedimentary models for rift-basin carbonate systems, *in* Lukasik, J., and Simo, T., eds., Controls on Carbonate Platform and Reef Development: SEPM, Special Publication 89, p. 83–105.

Cross, N.E., Bosence, D.W.J., and Purser, B.H., 1998, The tectono-sedimentary evolution of a rift margin carbonate platform: Abu Shaar, Gulf of Suez, Egypt, *in* Purser, B.H., and Bosence, D.W.J., eds., Sedimentation and Tectonics in Rift Basins: Red Sea–Gulf of Aden: London, Chapman and Hall, p. 271–295.

Crossley, R., and Cripps, D., 1999, Templates from mainland Africa and the Red Sea for interpreting the early evolution of the South Atlantic, *in* Cameron, N.R., Bate, R.H., and Clure, V.S., eds., The Oil and Gas Habitats of the South Atlantic: The Geological Society of London, Special Publication 153, p. 85–96.

Dorobek, S.L., 2008, Tectonic and depositional controls on syn-rift carbonate platform sedimentation, *in* Lukasik, J., and Simo, T., eds., Controls on Carbonate Platform and Reef Development: SEPM, Special Publication v. 89, p. 57–81.

Drummond, C.N., and Dugan, P.J., 1999, Self-organizing models of shallow-water carbonate accumulation: Journal of Sedimentary Research, v. 69, p. 939–946.

Dullo, W.-C., and Montaggioni, L., 1998, Modern Red Sea coral reefs: a review of their morphologies and zonation, *in* Purser, B.H., and Bosence, D.W.J., eds., Sedimentation and Tectonics in Rift Basins: Red Sea–Gulf of Aden: London, Chapman and Hall, p. 583–594.

Erlich, R.N., Barrett, S.F., and Guo, B.J., 1990, Seismic and geological characteristics of drowning events on carbonate platforms: American Association of Petroleum Geologists, Bulletin, v. 74, p. 1523–1537.

Erlich, R.N., Longo, A.P., and Hyare, S., 1993, Response of platform margins to drowning: evidence of environmental collapse, *in* Loucks, R.G., and Sarg, J.F., eds., Carbonate Sequence Stratigraphy: Recent Developments and Applications: American Association of Petroleum Geologists, Memoir 57, p. 241–266.

Fournier, F., Borgomano, J., and Montaggioni, L.F., 2005, Development patterns and controlling factors of Tertiary carbonate build-ups: New insights from high-resolution 3-D seismic and well data from the Malampaya gas field (Offshore Palawan, Philippines): Sedimentary Geology, v. 174, p. 189–215.

Fullmer, S., Kaczmarek, S.E., and Steffen, K., 2010, Modern carbonate facies: moving from description to quantitative prediction: 30th Annual Gulf Coast Section, SEPM Foundation, Bob F. Perkins Research Conference, Seismic Imaging of Depositional and Geomorphic Systems, December 5–8, 2010, Houston, Texas.

Grötsch, J., and Mercadier, C., 1999, Integrated 3-D reservoir modeling based on 3-D seismic: the Tertiary Malampaya and Camargo buildups, offshore Palawan, Philippines: American Association of Petroleum Geologists, Bulletin, v. 83, p. 1703–1728.

Guilcher, A., 1988, A heretofore neglected type of coral reef: The ridge reef. Morphology and origin: 6th International Coral Reef Symposium, Australia, Proceedings, v. 3, p. 399–402.

Gvirtzman, G., Buchbinder, B., Shen, A., Nir, Y., and Friedman, G.M., 1977, Morphology of the Red Sea fringing reefs a result of the erosional pattern of the last-glacial low-stand sea level and the following Holocene recolonization: Bureau Recherches Géologiques et Minières (France), Mémoires, no. 89, p. 480–491.

Hamouda, A.Z., and El-Wahhab, M.A., 2012, Detection of the bottom facies characteristics at El Zeit Bay, Red Sea, by using single-beam acoustic sound: Oceanology, v. 52, p. 60–71.

Haralick, R.M. and Shapiro, L.G., 1992, Computer and Robot Vision: Vols. 1, 2: Reading, Massachusetts, Addison-Wesley, 630 p.

Harris, P.M., and Vlaswinkel, B.M., 2008, Modern isolated carbonate platforms: templates for quantifying facies attributes of hydrocarbon reservoirs, *in* Lukasik, J., and Simo, T., eds., Controls on Carbonate Platform and Reef Development: SEPM, Special Publication 89, p. 323–341.

Harris, P.M., Ellis, J., and Purkis, S.J., 2011, Analyzing spatial patterns in modern carbonate sand bodies from Great Bahama Bank: Journal of Sedimentary Research, v. 81, p. 185–206.

Harris, P.M., Ellis, J., and Purkis, S.J., 2012, Analogs for carbonate deposition in early rift settings: SEPM, Short Course Notes 55, p. 1–75, and 2 DVDs.

Hofmann, P., Schwark, L., Brachert, T., Badaut, D., Riviere, M., and Purser, B.H., 1998, Sedimentation, organic geochemistry and diagenesis of cores from the axial zone of the southern Red Sea: relationships to rift dynamics and climate, *in* Purser, B.H., and Bosence, D.W.J., eds., Sedimentation and Tectonics in Rift Basins: Red Sea–Gulf of Aden: London, Chapman and Hall, p. 479–503.

Khalil, S.M., and McClay, K.R., 2002, Extensional fault-related folding, northwest Red Sea, Egypt: Journal of Structural Geology, v. 24, p. 743–762.

Mardia, K.V., and Jupp, P.E., 2000, Directional Statistics: Chichester, Wiley, 429 p.

Mitzenmacher, M., 2003, A brief history of generative models for power law and lognormal distributions: Internet Mathematics, v. 1, p. 226–251.

Montaggioni, L.F., Behairy, A.K.A., El-Sayed, M.K., and Yusuf, N., 1986, The modern reef complex, Jeddah area, Red Sea: a facies model for carbonate sedimentation on embryonic passive margins: Coral Reefs, v. 55, p. 127–150.

Orszag-Sperber, F., Harwood, G., Kendall, A., and Purser, B.H., 1998, A review of the evaporites of the Red Sea–Gulf of Suez rift, *in* Purser, B.H., and Bosence, D.W.J., eds., Sedimentation and Tectonics in Rift Basins: Red Sea–Gulf of Aden: London, Chapman and Hall, p. 409–425.

Perline, R., 2005, Strong, weak, and false inverse power laws: Statistical Science, v. 20, p. 68–88.

Pinsky, M.L., Palumbi, S.R., Andréfouët, S., and Purkis, S.J., 2012, Open and closed seascapes: where does habitat patchiness create populations with high fractions of self-recruitment?: Ecological Applications, v. 22, p. 1257–67.

Purkis, S.J., and Pasterkamp, J., 2004, Integrating *in situ* reef-top reflectance spectra with Landsat TM imagery to aid shallow-tropical benthic habitat mapping: Coral Reefs, v. 23, p. 5–20.

Purkis, S.J., and Vlaswinkel, B., 2012, Visualizing lateral anisotropy in modern carbonates: American Association of Petroleum Geologists, Bulletin, v. 96, p. 1665–1585.

Purkis, S.J., Kenter, J.A.M., Oikonomou, E.K., and Robinson, I.S., 2002, High-resolution ground verification, cluster analysis and optical model of reef substrate coverage on Landsat TM imagery (Red Sea, Egypt): International Journal of Remote Sensing, v. 23, p. 1677–1698.

Purkis, S.J., Riegl, B., and Andréfouët, S., 2005, Remote sensing of geomorphology and facies patterns on a modern carbonate ramp (Arabian Gulf, Dubai, U.A.E.): Journal of Sedimentary Research, v. 75, p. 861–876.

Purkis, S.J., Kohler, K.E., Riegl, B.M., and Rohmann, S.O., 2007, The statistics of natural shapes in modern coral reef landscapes: The Journal of Geology, v. 115, p. 493–508.

Purkis, S.J., Rowlands, G.P., Riegl, B.M., and Renaud, P.G., 2010, The paradox of tropical karst morphology in the coral reefs of the arid Middle East: Geology, v. 38, p. 227–230.

Rankey, E.C., 2002, Spatial patterns of sediment accumulation on a Holocene carbonate tidal flat, Northwest Andros Island, Bahamas: Journal of Sedimentary Research, v. 72, p. 591–601.

Rankey, E.C., 2004, On the interpretation of shallow shelf carbonate facies and habitats: how much does water depth matter?: Journal of Sedimentary Research, v. 74, p. 2–6.

Reinicke, G.B., Kroll, D.K., and Schuhmacher, H., 2003, Patterns and changes of reef-coral communities at the Sanganeb-Atoll (Sudan, Central Red Sea): 1980 to 1991: Facies, v. 49, p. 271–298.

Rowlands, G., Purkis, S.J., Riegl, B., Metsamaa, L., Bruckner, A., and Renaud, P., 2012, Satellite imaging coral reef resilience at regional scale. A case-study from Saudi Arabia: Marine Pollution Bulletin, v. 64, p. 1222–1237.

Shannon, C.E., and Weaver, W., 1962, The Mathematical Theory of Communication: Urbana, University of Illinois Press, 144 p.

Stumpf, R.P., Holderied, K., and Sinclair, M., 2003, Determination of water depth with high-resolution satellite imagery over variable bottom types: Limnology and Oceanography, v. 48, p. 547–556.

Turak, E., Brodie, J., and Devantier, L., 2007, Reef-building corals and coral communities of the Yemen Red Sea: Fauna of Arabia, v. 23, p. 1–40.

Wilkinson, B.H., Drummond, C.N., Diedrich, N.W., and Rothman, E.D., 1999, Poisson processes of carbonate accumulation on Paleozoic and Holocene platforms: Journal of Sedimentary Research, v. 69, p. 338–350.

Received 30 January 2012; accepted 17 September 2012.